ROLE OF METASTABLE PITTING IN CREVICES ON CREVICE STABILIZATION IN ALLOYS 625 AND 22

B.A. Kehler and J.R. Scully
Center for Electrochemical Science and Engineering
Department of Materials Science and Engineering
University of Virginia
Charlottesville, VA 22904

ABSTRACT

The metastable pitting behavior inside crevices of alloys 625 and 22 was examined to obtain insight into differences in crevice corrosion susceptibility between alloys 625 and 22. Metastable corrosion event rates recorded as current-time transients were found to increase with increasing applied potential and temperature for both alloys. However, the increase was more significant for 625 as compared to alloy 22 and the cumulative number of events was greater. A strong correlation was obtained between the increase in event rates and decrease in crevice stabilization potential with temperature. Metastable peak heights, values for peak integrated charge, and current/pit depth (I/r) ratios were not strongly affected by these driving forces. The alloying content in alloy 22, traced to increased molybdenum (Mo) and tungsten (W), was rationalized to decrease the metastable event rate and hence, the cumulative number of events after a given time. However, metastable peak heights, values for peak integrated charge, and I/r ratios, as well as metastable peak shapes associated with individual events, were not strongly affected by alloy type in the narrow range of Mo contents explored here. Observed differences in resistance to crevice corrosion stabilization are rationalized to depend on differences in the cumulative number of metastable events occurring sufficiently close in space and time to contribute to the development of a critical crevice chemistry at specific depths in a crevice. The properties of individual events did not have a significant effect. Stable crevice corrosion eventually occurred at the sites where a row of metastable pits formed at a critical distance from

the crevice mouth. This row of pit sites focused acidification, which contributed to local depassivation.

KEY WORDS: crevice corrosion, metastable pitting, 625, alloy 22

INTRODUCTION

Stable Crevice Corrosion Properties of Alloys 625 and 22

Alloy 22 with a pitting resistance equivalency number (PREN)[(1)] of 65 is markedly more resistant to crevice corrosion than 625 with a PREN of 50.[1] Previous studies have shown that electrolyte ratio (i.e., the ratio of chloride anions to total oxyanions) and temperature have a strong effect on calculated survival probabilities and crevice generation rates for both alloys 625 and 22.[2] In addition, multiple regression analysis showed that the crevice stabilization potential, E_{crev}, is a stronger function of temperature and electrolyte composition for alloy 22 than for 625. As temperatures are lowered from 95°C, E_{crev} values increase more rapidly for alloy 22 than for 625, in some instances approaching or exceeding transpassive potentials.[2] In addition, critical crevice temperature studies in 6% ferric chloride ($FeCl_3$) showed that crevice corrosion initiated at lower temperatures for 625 than for alloy 22.[3] Hence, crevice corrosion susceptibility in 625 is far greater than in alloy 22, but the exact reasons for such susceptibility are unknown.

Transition to Stable Crevice Corrosion

Laycock, et al., suggest four possible models for the stabilization of crevice corrosion.[4] The passive dissolution model is based on a mechanism suggested by Oldfield and Sutton in which the formation of a critical environment leads to the local breakdown of the passive film and thus, general corrosion in that area.[5, 6] In the sulfide entrapment model, dissolution of evenly spaced inclusions concurrent with passive dissolution leads to the breakdown of the passive film.[7, 8] The IR drop model is based on a mechanism suggested by Pickering where the IR drop

---

[(1)] PREN = wt.%Cr + 3.3wt.%Mo +16wt.%N.

in the restricted geometry is sufficient to alter the interfacial potential within the crevice from the passive region into the active region, thereby, initiating crevice corrosion.[9-12] Finally, in the metastable pitting model of Stockert and Boehni, pitting is stabilized due to the geometrical restrictions of the crevice in which ohmic potential drop and restricted mass transfer maintain the active state caused by a metastable pit.[13]

Metallurgical Considerations

Numerous studies have examined the effect of alloying additions on the pitting properties of stainless steels.[14-18] Sedriks has suggested that structural heterogeneities that influence pitting may also influence crevice corrosion. For example, manganese sulfide (MnS) inclusions and chromium depleted zones around precipitated carbides have been found to be initiation sites for metastable pitting that may transition to stable pits. These sites may also act as initiation sites for crevice corrosion.[1]

The materials of this study, alloys 625 and 22, have single-phase face-centered cubic (FCC) atomic structures similar to austenitic stainless steels.[19] Standard heat treatments of these alloys[(2)] lead to the desired single-phase atomic structure despite differences in cooling rates. However, second phases including carbides and intermetallics can be formed under certain thermal conditions. Long term aging at intermediate temperatures (approximately 600°C) leads to the precipitation of carbides as well as a μ phase that nucleates from the carbides at the grain boundaries.[20]

In addition, alloying additions such as Mo and W used to enhance corrosion resistance and strength can form carbides and intermetallics. For 625, carbides can be found in the form MC or M_6C where M is Ni, Nb, or Mo. The intermetallic Ni_3Nb can also form. The μ phase

---

[(2)] Alloy 625 was tested in a mill-annealed condition (furnace cooled) and alloy 22 was tested in a solution-annealed condition (water quenched).

consisting of Ni, Mo, Cr, W, and Fe can form in alloy 22. Precipitation of the σ and P phases can also occur in these high nickel alloys.[1, 21, 22] However, Mo and W are more soluble at temperatures above 1000°C than at lower temperatures.[19] Therefore, the solution heat treatment and water quenching (or furnace cooling) ensure retention of these elements within the single-phase FCC structure. In fact, studies of aging and phase stability studies on alloy 22 show that formation of P or σ phases is unlikely at 200°C for over 10,000 years.[23] Therefore, the metallurgical culprits responsible for pitting and crevice corrosion of alloys 625 and 22 are less clear than in the case of MnS inclusions in stainless steels.

Justification for Investigating the Role of Pitting in Crevice Corrosion

Metastable pitting behavior inside crevices was studied for a variety of reasons. First, many potential long-term application, such as in high level nuclear waste containment at Yucca Mountain, could benefit from clearer understand of metastable pitting.[20,24,25] If the metastable event rate is sufficiently high and does not decay with time, an engineering structure could conceivably be breached due to coalescence and penetration of metastable pit sites despite the fact that stabilization has not occurred. Even if metastable pit sites do not coalesce nor penetrate an engineering structure, metastable pitting can shed additional information regarding the factors that control pit of crevice stabilization. For instance, it has been suggested that crevice stabilization will eventually occur given enough time if the metastable pitting rate does not decay to zero with time due to the role of the restricted geometry of the crevice in maintaining an aggressive chemistry.[4] Hence, any potential where long term metastable pitting occurs may be a potential where crevice stabilization might occur given severe enough mass transport conditions. Metastable events may contribute to crevice stabilization through their influence on chemistry change by means other than passive dissolution. In the context of Galvele's chemistry change

proposal for stabilization,[17] studies have shown that there exists a critical value of i*r or I/r, where i is pit current density, I is pit current, and r is pit depth, that is required to maintain a depassivating chemistry and therefore, stabilize pits.[15, 26, 27] In the context of crevice corrosion, r must include the crevice depth as an additional geometric restriction to mass transport. Metastable events may also contribute to crevice stabilization by providing IR drop in the context of ohmic models of crevice stabilization.[9-12, 28, 29] Metastable events can also be correlated with the probability of stable crevice corrosion based on a probabilistic model developed by Shibata.[30] This stochastically based model, which involves the determination of birth, death, and stable growth rate expressions, has been applied in metastable pitting studies to predict damage evolution.[15, 31] Thus, the mechanism of crevice corrosion can be better understood by studying the stages of the process, i.e., initiation, growth, and repassivation.[14] Here, we focus on the initiation stage involving metastable events.

Many researchers have examined metastable localized corrosion properties, specifically the metastable pitting properties of stainless steels[14, 26, 32, 33] and aluminum alloys[26, 27, 34] through potentiostatic holds in the passive region. Metastable events have been observed at potentials well below potentiodynamically determined pitting potentials,[15, 32] as well as below repassivation potentials.[15, 27, 35] Also, an exponential decay in the number of metastable events with time, at fixed potential and temperature, has been observed and has been attributed to the elimination of possible sites for pitting events.[26, 33] In addition, Stockert and Boehni examined the influence of metastable pitting on the formation of stable crevices. Their studies showed that stable crevice corrosion could be initiated only after the occurrence of a certain number of metastable pitting events, which contributes to the formation of a depassivating chemistry.[13]

Studies involving an examination of metastable pit sites inside crevices are significant because alloys 625 and 22 without crevices resist stable pitting in many environments. Therefore, measurements of metastable pit event rate, peak height, peak integrated charge, and I/r ratios, as well as examination of the growth and repassivation, could lead to a better understanding as to why the crevice corrosion resistance of alloy 22 is better than 625 from the standpoint of crevice initiation and what alloy design considerations improve crevice corrosion resistance. In this study, the effects of temperature and applied potential on metastable pit sites within crevices are examined in order to investigate the role of metastable pitting in crevice corrosion stabilization, and to examine the connection between crevice corrosion stabilization and metastable corrosion properties.

Objectives

The main objectives of this study are to compare and contrast the metastable pitting behavior inside crevices of alloys 625 and 22 and to determine the extent to which these properties are linked to and provide mechanistic information on the greater overall crevice corrosion resistance of alloy 22 relative to 625. Potentiostatic studies were performed to determine the effects of temperature and applied potential on metastable pitting inside crevices of alloys 625 and 22 given the distinct differences in crevice corrosion behavior of these two alloys. Current versus time behavior characterized in terms of event rate, peak integrated charge, and peak shape was examined. Analyzed data include I/r ratios, repassivation rates, and cumulative number of events. In addition to analysis of current-time records, surface metrology studies were performed to compare the nature, location, and extent of metastable surface damage with the corresponding electrochemical current versus time behavior.

EXPERIMENTAL PROCEDURES

Materials

Metastable pitting behavior inside crevices of alloys 625 and 22 was investigated through analysis of current-time records using specimens with an as-received surface finish of between 2 and 4 μm (average roughness) arranged in a crevice assembly. Prior to testing, the specimens, which had been stored in laboratory air for six months or more, were degreased in acetone, rinsed in deionized water, and dried at 100°C for three minutes in accordance with ASTM-G1.[36] The face of the sample was placed inside a crevice assembly consisting of ceramic multiple crevice formers with 12 plateaus each of area 0.06 cm² lined with polytetrafluoroethylene (PTFE) tape. The torque applied was 7.92 N-m (70 in-lb). The total wetted area of each specimen was approximately 8.5 cm² including both the sample face and stem, but the only crevice was formed by the crevice former on the face of the sample.

Surface metrology studies were performed using alloys 625 and 22 in a polished condition to better facilitate detection of geometrically small corrosion events such as metastable pits. Polished samples were wet polished through 600 grit SiC paper and successively polished to a 1 μm diamond finish in stages of 6 μm, 3 μm, and 1 μm diamond slurry, and stored in laboratory air for at least 8 hours before testing. Prior to testing, the samples were degreased in acetone, rinsed in deionized water, and dried at room temperature. The alloy compositions and specifications are shown in Table 1[37] and Table 2, respectively. Shown in Table 3 are characteristic values for chromium equivalencies,[38] pitting resistance equivalency numbers,[1] and modified pitting resistance equivalency numbers,[39] which are indicative of the relative corrosion resistance of these alloys.[(3)]

[(3)] PREN = wt.%Cr + 3.3wt%Mo +16wt.%N; PRE' = wt%Cr +3.3wt.%(Mo + W) + 30wt.%N; Cr Equivalency = wt.%Cr + 1.6wt.%Mo + 4.3wt.%Nb + 7wt.%W.

Electrochemical Testing Methods

Previous studies have characterized the potential ranges of passivity for alloys 625 and 22 in different environments through examination of potentiodynamically determined potentials for crevice stabilization, repassivation, and free corrosion.[2] In order to examine the metastable pitting behavior inside crevices of these alloys potentiostatic holds were performed at a data acquisition rate of 20 Hz. This data acquisition rate was considered sufficient to capture the shape of the transient corrosion events. Potentials were chosen in the passive region above open circuit but well below those associated with stabilization in order to avoid the transition to stability at short times. Potentiostatic holds were performed for 10 hours (or until stabilization of crevice corrosion occurred) at temperatures ranging from 60° to 95^oC in a pH 2.75 (10:1) electrolyte, where (10:1) indicates the ratio of chloride anions (5 M lithium chloride) to total oxyanions (0.26 M sodium sulfate and 0.24 M sodium nitrate). The pH was adjusted to 2.75 with hydrochloric acid (HCl) to a final concentration of 0.2 mM HCl.[(4) 38] This electrolyte was chosen over a higher pH environment in order to give a large potential range between the applied potentials and thermodynamic potentials associated with chromium and molybdenum transpassivity. The applied potentials in millivolts versus Ag/AgCl (25^oC) were –25 and +5. All experiments were performed using the same potentiostat (Princeton Applied Research Model 273) and the same reference electrode in order to eliminate variations in measurements caused by slight equipment differences. Noise was minimized by performing all experiments in a Faraday cage and isolating the cell from the heat source by circulating heated water through a coil placed directly in the cell. In addition, an internal 590 Hz low pass filter was employed to eliminate high frequency noise and the internal measurement rate of the potentiostat was set at 240 Hz to help cancel 60 Hz power line interference.[40, 41] The ground lead from the electrometer was used

---

[(4)] For electrolytes with high chloride concentrations, the activity coefficient of H^+ is greater than one.

to establish ground with the Faraday cage, thereby eliminating noise due to ground loop interference.[40] The test setup is shown in Figure 1.

Metastable corrosion event rates, peak heights, values for peak integrated charge, and I/r ratios were determined from current-time records using PeakFindC analysis software.[42] PeakFindC defines a metastable corrosion event based on a user input of threshold current, which establishes the difference between metastable events and background noise. Outputs of PeakFindC include metastable peak height, width, and integrated charge with a corresponding time stamp. Peak widths are determined at a current equivalent to 10% of the corresponding peak height. Values for peak integrated charge are calculated assuming that the events are triangular in shape, yielding a rough approximation of the charge passed during each event. It should be noted that PeakFindC assumes a baseline current level of zero. Therefore, in order to analyze the current-time records produced as a result of this study where the baseline current was not zero, the first 10,000 seconds of the current-time records were fit to a power law function. This yielded a good approximation of the initial decay of the current to the baseline current level (i.e., the passive current). This function was then subtracted from the original data file yielding a current-time record with a baseline current level of approximately zero.

The appropriate current threshold for counting of metastable events was determined by collecting current versus time records for 625 in both an aggressive chloride electrolyte and a benign phosphate electrolyte. Specifically, potentiostatic holds of +5 mV$_{Ag/AgCl}$ were performed in a pH 2.75 phosphate buffer at 95°C on uncreviced samples of 625 and compared to the results for creviced specimens of 625 polarized to +5 mV$_{Ag/AgCl}$ in the pH 2.75 (10:1) electrolyte at 95°C. The signal collected in the chloride electrolyte includes true metastable events and background noise, while the signal collected in the benign phosphate electrolyte includes only

background noise. Therefore, the appropriate current threshold for counting metastable events was determined through comparison of these two signals. The current-time records were examined using current thresholds ranging from 1 nA to 100 nA in 1 nA increments to determine the total number of events detected at each threshold. Figure 2 shows the current versus time records for the phosphate and chloride electrolytes, as well as results of the current threshold examination. If the selected current threshold is too low, the total number of events for each condition will be similar because erroneous event counting from the background noise is included in determination of metastable events. However, at a particular current threshold, the number of events counted for the chloride electrolyte exceeds those for the phosphate electrolyte, as the number of events detected that are actually just background noise begins to decrease. This is shown by the solid vertical line in Figure 2b. For the purpose of this study, the threshold current for counting metastable events was defined as the current at which the total number of events in the benign phosphate electrolyte was less than 10% of the total number of events in the chloride electrolyte and is indicated by the dotted vertical line in Figure 2b. This leads to the determination of true metastable events without a significant influence from background noise and artifact events. A current threshold of 56 nA was selected based on this procedure for all analyses in this study. However, this does not imply that metastable events below this threshold do not exist.[14] Smaller electrodes and smaller crevice areas would be required to acquire this data.

Selected metastable events were also examined to gain an understanding of growth and repassivation kinetics. The influence of peak shape on the electrochemical processes of growth and repassivation was investigated by examining the peaks of greatest height, determined using PeakFindC, at each condition tested (i.e., each temperature and potential combination) for both

alloys. These selected events were characterized largely on the basis of event lifetimes. In addition, repassivation kinetics were analyzed through examination of metastable events of similar peak heights using modified current-time records with an approximate baseline current of zero. It was assumed that current versus time behavior during the repassivation stage follows a power law such that $I = \alpha t^m$.[43] For the purpose of repassivation analysis, several assumptions were made and are illustrated in Figure 3. First, the initiation of a metastable event corresponds to time zero in the lifetime of the event.[44] Second, the passive current is defined as the current at time zero. Third, the event is considered complete when the current returns to or drops below the level of the passive current. Applying these assumptions discussed above, power law fits of the repassivation stage were performed after subtraction of the passive current from each data point in the repassivation stage such that the modified passive current was zero yielding m-values characteristic of the repassivation kinetics.

Surface Metrology

Confocal laser scanning microscopy (CLSM) was used to correlate metastable signals from potentiostatic holds with surface features and to examine the evolution of crevice corrosion. Polished samples were tested potentiostatically at +5 $mV_{Ag/AgCl}$ at 95°C in the pH 2.75 (10:1) electrolyte for accumulated anodic charges of 0.005 C, 0.01 C, and 0.02 C.[5] These quantities correspond to metastable corrosion (i.e., stabilization has not yet occurred), just after stabilization, and stabilization followed by a short period of propagation of crevice corrosion, respectively, and are indicated in Figure 4 as arrows 1, 2, and 3, respectively. Additional studies were conducted on samples held potentiostatically at +400 $mV_{Ag/AgCl}$ for an accumulated anodic charge of 4 C to further characterize the propagation stage. Samples were characterized by

---

[5] These quantities were chosen through examination of the current-time records from potentiostatic hold experiments and were adopted as consistent, though somewhat arbitrary, criteria for metastable corrosion, just after stabilization, and stabilization followed by a short period of propagation.

reflected light intensity maps and 3-D depth profiles converted to gray scale after each time interval in order to determine the extent of damage after accumulation of controlled consistent quantities of anodic charge and to investigate the transition to stability in terms of location and extent of surface damage.

RESULTS

Correlation between Metastable Pitting in Crevices and Crevice Stabilization

In this study, the effects of temperature and applied potential on metastable pitting behavior inside crevices were explored in pH 2.75 (10:1) electrolyte where (10:1) indicates the ratio of chloride anions to total oxyanions. In this electrolyte at $95^{\circ}C$ the average crevice stabilization potentials were 236 $mV_{Ag/AgCl}$ and 357 $mV_{Ag/AgCl}$ for alloys 625 and 22, respectively. The average repassivation potentials were -101 $mV_{Ag/AgCl}$ and 158 $mV_{Ag/AgCl}$ for alloys 625 and 22, respectively.[6] 2

There is a correlation between the cumulative number of metastable events formed at a fixed potential and temperature and, thus, the crevice stabilization parameter, E_{crev}, at the same temperature. Figure 5 shows that the cumulative number of events recorded at +5 $mV_{Ag/AgCl}$ (a) and -25 $mV_{Ag/AgCl}$ (b) increased with increasing temperature corresponding to a decrease in E_{crev} with increasing temperature. Figure 5 also shows that for each temperature, there are a greater number of events for 625 than for alloy 22. This correlates with lower E_{crev} values at each temperature for 625 as compared to alloy 22. Therefore, temperature has an effect on both metastable pit rates and stable crevice corrosion potentials.

---

[6] E_{crev} and $E_{r,crev}$ values were calculated using formulas developed through multiple regression analysis from previous potentiodynamic studies using at least 5 replicate specimens for each condition tested. These formulas related potential (E_{crev} or $E_{r,crev}$) as a function of temperature and electrolyte ratio.

Electrochemical Characterization of Metastable Pitting Events in Crevices

Figure 6 and Figure 7 show the effect of temperature on the cumulative number of metastable pitting events in crevices[7] for alloys 625 and 22 with corresponding metastable event rates at applied potentials of +5 mV$_{Ag/AgCl}$ and −25 mV$_{Ag/AgCl}$, respectively. These potentials are more negative than potentiodynamically determined stabilization potentials and more positive than potentiodynamically determined repassivation potentials for 625. Through these figures, it can be seen that the number of events detected decays with time for both alloys. A large number of metastable events are detected in the first 5,000 seconds of each current-time record. The number of new metastable events decreases with time, leading to a decrease in the metastable event rate. In addition, the figures illustrate that the number of metastable events detected and the event rate tend to increase with increasing temperature. Figure 6 and Figure 7 also show that metastable event rates increase with temperature and that metastable event rates are slightly higher for 625 than for alloy 22. It should be noted that crevice corrosion stabilization occurred at 95°C at times ranging from 9,000 to 25,000 seconds even after a marked decrease in the number of new events with time indicating that the cumulative number of events was more likely to play a role in crevice stabilization rather than a single trigger event. Applied potential also has an effect on the cumulative number of events and the event rate. An applied potential of +5 mV$_{Ag/AgCl}$ usually leads to an increased metastable event rate as compared to −25 mV$_{Ag/AgCl}$.

Metastable pitting events in crevices were also characterized through analysis of metastable peak heights, values for peak integrated charge, and I$_{peak}$/r ratios. Figure 8 presents cumulative probabilities (CPs) for distributions of metastable peak heights for alloys 625 and 22 at applied potentials of +5 and -25 mV$_{Ag/AgCl}$. The distributions range from approximately 2x10^{-8}

---

[7] Metastable pitting events were only seen in creviced alloy 22 and 625 samples. These events were consistent with metastable pitting events seen in stainless steels. Hereafter, the term "metastable event" is used to describe metastable pitting events within crevices.

A (1% CP) to 7×10^{-6} A (99% CP) and are similar for the two alloys. Figure 9 presents CPs for distributions of values for peak integrated charge for alloys 625 and 22. The peak integrated charge distributions for alloys 625 and 22 are overlapping in each case and do not exhibit a discernible potential dependence for $\Delta E = 30$ mV (i.e., between $-25_{Ag/AgCl}$ and $+5$ mV$_{Ag/AgCl}$). Values for peak integrated charge recorded range from approximately 6×10^{-10} C (1% CP) to 2×10^{-6} C (99% CP), corresponding to metastable pit radii of roughly 0.21 μm to 3.1 μm, assuming a hemispherical pit geometry and negligible cathodic reactions in pits, which is likely. Figure 10 presents CPs for distributions of I_{peak}/r ratios for alloys 625 and 22. The distributions range from approximately 4×10^{-4} A/cm (1% CP) to 2×10^{-2} A/cm (99% CP) and are also similar for the two alloys.

The data indicate (Figure 8 through Figure 10) that there is minimal difference between alloys 625 and 22 in metastable peak heights, values for peak integrated charge, and I/r ratios for a large population of events. However, there may be a difference in the shape of these metastable events, which could yield information regarding growth and repassivation kinetics. The influence of peak shape on the electrochemical processes of growth and repassivation was investigated by examining selected metastable events at each condition tested (i.e., each temperature and potential combination) for both alloys.

Metastable event shapes were initially examined through analysis of the metastable events of greatest peak height for alloys 625 and 22 at temperatures of 60°, 80°, and 95°C polarized to $+5$ mV$_{Ag/AgCl}$ and -25 mV$_{Ag/AgCl}$, respectively. Both alloys exhibit cases where there is an abrupt increase in current followed by either an abrupt decrease or a slow decay, as well as cases where there is a gradual increase in current followed by a gradual decrease. "Non-damage events" occur with lifetimes less than one second or with immediate repassivation indicating

minimal propagation. In addition, events occur over larger time periods where there is propagation after the initial increase in current and possibly the immediate initiation of another metastable event. These, so-called "damage events", have been seen elsewhere.[45]

Metastable event shapes were examined further through analysis of repassivation rates for non-damage events of peak currents ranging from 0.10 to 0.16 μA. However, no significant difference between the repassivation kinetics of alloys 625 and 22 was detected.

Characterization of Surface Metrology

The progression of crevice corrosion was examined through confocal laser scanning microscopy (CLSM) of surfaces corresponding to the detection of metastable events only, the initiation of stable crevice corrosion, and the propagation of stable crevice corrosion.

CLSM images of polished 625 and alloy 22 surfaces are shown in Figure 11 as a comparison to surfaces associated with a finite accumulated anodic charge. Note that each polished surface contains several micron sized dimples, possibly due to embedded particle pull-out.

Figure 12 and Figure 13 show 2-D CLSM images of 625 and alloy 22 surfaces, respectively, after a charge accumulation of 0.005 C. The figures reveal the occurrence of independent micron-scale damage or pits of dimensions consistent with the charge associated with metastable events. These sites are found inside crevices and are not observed on surfaces outside crevices, which is consistent with electrochemistry on uncreviced specimens. Assuming hemispherical geometry, values for peak integrated charge are associated with pit sizes of approximately 0.21 μm (1% CP) to 3.1 μm (99% CP).[8] These pits coalesce leading to a narrow band of attack within the crevice region. According to the current-time record (Figure 4), this

---

[8] Values quoted are from the analysis of current-time records using specimens with an as-received surface finish of between 2 and 4 μm (average roughness).

narrow band of attack is not associated with stable crevice corrosion. Also, note that micron scale indications seen away from this band of attack, either within the crevice region or on the bold surface, can most likely be associated with surface defects caused by polishing as seen in Figure 11 because the area density of similar defects is the same.

Figure 14a presents a 2-D CLSM image of 625 after an accumulated anodic charge of 0.01 C revealing two regions of attack. The region closest to the outer edge of the crevice region corresponds to etch attack and is likely associated with intergranular corrosion (IGC) as the geometry of attack corresponds roughly to the average grain size of 625 (approximately 22 μm).[46] A slight roughening effect is seen for the region of etch attack as compared to the bold surface. The second region of attack lies farther into the crevice region beyond the area of etch attack and is characterized by a pronounced depth of attack. In addition, a 2-D CLSM image of alloy 22 shown in Figure 14b after an accumulated anodic charge of 0.01 C also revealed evidence of etch attack and possibly IGC. The average grain size of alloy 22 is approximately 45 μm corresponding to the geometry of attack.[46] However, there is no region of deep attack for alloy 22.

The crevice corroded surface for 625 after a short period of propagation of stable crevice corrosion is shown in Figure 15. This corresponds to an accumulated anodic charge of 0.02 C. The figure illustrates a pronounced depth of attack under the crevice former but near the crevice mouth that did not become deeper at greater depths into the crevice region. This may correspond to the mechanism of cathodic focusing where the crevice is unable to corrode deeper.[28] Therefore, the results suggest that the region of etch attack (corresponding to the initial region of metastable attack) seen in Figure 14a has progressed to a region of deep attack. Again, this deep attack is never seen for alloy 22. After propagation with further charge accumulation,

examination of the alloy 22 surface (not shown) reveals further damage due to etch attack, but no pronounced depth of attack at any site in the multiple crevice assembly.

This deep attack seen in alloy 625 at 0.01 C and 0.02 C of accumulated anodic charge is also seen after propagation of stable crevice corrosion. Figure 16 presents 3-D CLSM images of alloys 625 and 22 after an accumulated anodic charge of 4 C. The images reveal deeper attack for alloy 625 (120 μm) than for alloy 22 (45 μm).

DISCUSSION

Mechanism for Crevice Stabilization

Experimental results show that metastable event rates and hence, the cumulative number of events within a crevice, are greater for 625 than for alloy 22. In addition, the effect of temperature on metastable event rate is clarified through Figure 6 and Figure 7 where it is seen that metastable event rates increase to a greater extent with increasing temperature for 625 compared to alloy 22. Applied potential was also found to affect metastable event rates as the higher applied potential led to higher metastable event rates in most cases. Williams, et al., examined metastable pitting and its effect on the transition to stability for 304L and 316L stainless steels.[15] It was concluded that the probability of stable pitting (i.e., the formation of a propagating pit) is related to the probability of metastable pit initiation. Therefore, the probability of stable pitting should approach zero as the metastable event rate approaches zero. This was also observed by Scully, et al., in studies of metastable pitting of 316L stainless steel and high purity aluminum.[26] The rationale was that the number of metastable events decreased with time such that the metastable event rate approached a very low level beyond a time, t, where t is the time at which there are no available corrosion sites left.[26, 33] In the present study, crevice stabilization occurred at 95°C despite the fact that detected metastable event rates approached

zero.[9] The observation that stabilization occurs despite the fact that metastable event rates approach very low levels (and possibly zero) suggests that local chemistry change due to focused metastable pitting dominates the transition to stabilization of crevice corrosion rather than the crucial amount of ohmic potential drop brought about by an individual metastable event.

A more detailed analysis supports this point. IR voltage drop is necessary when an active/passive transition occurs such as in the case of alloys 625 or 22 in a strong reducing acid. Let us consider quantitatively the IR voltage drop from both passive dissolution and metastable pitting. Figure 17 shows anodic polarization curves for uncreviced 625 and alloy 22 specimens in HCl solutions of increasing molarity. Increasing HCl molarity leads to a greater I_{peak} for 625 compared to alloy 22. Thus, stabilization of crevice corrosion in alloy 22 requires a more aggressive crevice environment in addition to IR drop. In other words, the IR contribution from a metastable pit alone is not sufficient to lead to stabilization through the IR* model without significant local chemistry change. In addition, the plots show that IR* for 625 is approximately 150 mV for an applied potential of +5 mV$_{Ag/AgCl}$ when i_{pass} is 10^{-4} A/cm^2 (1 M HCl).

Consider ohmic potential drop due to passive current density alone. At a distance x into the crevice ohmic potential drop is given by Equation 1:[47]

$$V_{\Omega} = \frac{1}{w} \int_0^x \rho(x) \left[\int_x^L i(x)\,dx \right] dx \qquad \text{Equation 1}$$

where i(x) is the current density flowing into the crevice electrolyte, w is the crevice gap (10^{-5} cm), $\rho(x)$ is the solution resistivity (estimated by Shaw, et al., to be 7.5 Ω cm for alloy 625)[48], and L is the total crevice depth. It is assumed that $\rho(x)$ changes negligibly in the concentrated electrolyte of the crevice solution given the opposing influences of increased concentration and

---

[9] Metastable event rates only include events at a current threshold of 56 nA. Because of this threshold level, small nucleation events were not included in metastable event rate calculations leading to the observation that large event rates decay with time in all cases.

decreased ionic mobility in non-dilute solutions with concentration.[49] Thus, assuming passive

current density, i_{pass}, is the only contribution to ohmic drop and i_{pass} is constant within the crevice

region, V_Ω is given by Equation 2:[47]

$$V_\Omega = \frac{\rho}{w} \int_0^x i_{pass}(L-x)\,dx = \frac{\rho}{w} i_{pass}\left(Lx - \frac{1}{2}x^2\right) \qquad \text{Equation 2}$$

The representation of the crevice geometry shown in Figure 18 reveals three

contributions to ohmic potential drop over the distances d, x_{crit}, and 2r where $L \approx d + x_{crit} + 2r$.

The distance d is the distance between the remotely located reference electrode and the edge of

the crevice former. For a well supported electrolyte, ohmic drop over the distance d is

negligible. The distance x_{crit} is the distance into the crevice region at which metastable pitting

occurs. The distance 2r is the diameter of the metastable pit formed and will be considered later.

Thus, ohmic drop at the crevice depth, x_{crit}, due to passive current density alone occurs over a

distance x_{crit} (i.e., $x = L = x_{crit}$) and is given by Equation 3:

$$V_\Omega = \frac{\rho}{w} i_{pass}\left(\frac{1}{2}x_{crit}^{\,2}\right) \qquad \text{Equation 3}$$

Now consider the contribution of a small metastable pit to ohmic potential drop. The equation

for V_Ω now takes into account the additional current due to the metastable pit (I_{peak}) and is given

by Equation 4:

$$V_\Omega = \frac{\rho}{w}\left[\int_0^{x_{crit}} i_{pass}(L-x)\,dx + \int_{x_{crit}}^{x_{crit}+2r} \frac{I_{peak}}{A_{slice}}(L-x)\,dx \right] \qquad \text{Equation 4}$$

where $A_{slice} = 0.25\,(2r)$ cm^2 (the rectangular slice of the crevice within which the metastable pit

occurs; Figure 12 and Figure 13) and $L \approx x_{crit} + 2r$. The equation assumes that the contribution

from i_{pass} over A_{slice} is negligible compared to that of the metastable pit current. Figure 19 shows

the effect of i_{pass} on V_Ω considering contributions from i_{pass} only and i_{pass} plus the formation of

metastable pits at a depth x_{crit} corresponding to cumulative probabilities (CPs) of 99%, 50%, and 1% for experimentally measured metastable peak heights and values for peak integrated charge. Assuming the CP curves follow a Gaussian distribution, metastable events corresponding to CPs of 99% and 1% are considered rare events, while those corresponding to a CP of 50% are the most likely. Thus, calculations corresponding to CPs of 99% and 1% yield the range of possible values for V_Ω, while calculations corresponding to a CP of 50% yields the most likely value of V_Ω. Figure 19 reveals that the formation of a metastable pit at a depth L increases V_Ω by approximately 7 mV for a large metastable pit (99% CP) and approximately 1 μV for a small metastable pit (1% CP). An intermediate metastable pit (50% CP) increases V_Ω by approximately 33 μV. Thus, the contribution of the most likely single metastable pit to ohmic potential drop is negligible for all values of passive current density.

V_Ω is controlled by the contribution from passive current density at a value of i_{pass} that is dependent on the magnitude of the contribution to V_Ω due to a metastable pit. For example, Figure 19 shows that V_Ω increases significantly at passive current densities above 10^{-3} A/cm^2 for large metastable pits (99% CP), whereas V_Ω is controlled by i_{pass} over all values of i_{pass} for small metastable pits (1% CP). Recall that IR* for 625 is approximately 150 mV for an applied potential of +5 mV$_{Ag/AgCl}$ when i_{pass} is 10^{-4} A/cm^2 (1 M HCl). Thus, the formation of a metastable pit at a depth L in this situation would not create the required ohmic potential drop required for crevice stabilization in an aggressive 1 M HCl crevice environment. Ohmic potential drop is dominated by the contribution from passive current density and stabilization would not occur without a large increase in passive current density. Thus, the role of a single event in satisfying the IR>IR* criterion could be questioned. It seems more likely that metastable events contribute to local acidification by metal ion hydrolysis, which causes an

increase in the local passive current (I_{pass}). In studies of high Cr-Mo alloys, Lillard, et al., observed that a severe environment was required to create the necessary local increase in I_{pass} and thus enable initiation of crevice corrosion through the IR* mechanism.[38]

It is also likely that crevice stabilization is not caused by a single event meeting the i*r criterion in the context of Galvele's model for pit stabilization[17] as the event with the largest I/r ratio did not occur immediately before stabilization in a systematic manner. Recognizing that the crevice depth must be considered in any estimation of critical I/r ratio, either the Galvele criterion[17] must be rewritten to account for a crevice depth of x, or the solution concentration within the crevice at the mouth of the metastable pit needs to be considered. Assuming the former case, the simple Galvele criterion, neglecting passive dissolution over the length L, and neglecting transport by migration, becomes:

$$\frac{I}{2\pi r}\left(1 + \frac{x}{r}\right) = nFDC_s \qquad \text{Equation 5}$$

where C_s is the concentration at the pit bottom which must be maintained above the critical concentration, typically taken as near the saturation concentration in order for crevice attack to stablize. Unfortunately, x is unknown but two scenarios may be envisioned. If x~r then I/r needs to be about the same as in the case of pitting without a crevice all other things being equal. If x>>r, then the I/r ratio required for pit stabilization might drop below 10^{-2} A/cm. Indeed, it is seen that the I/r criterion of 10^{-2} A/cm, observed for pitting of stainless steel,[26] is transiently obtained in some of the metastable pit events for alloys 625 and 22 at temperatures less than 95°C (Figure 20). However, the 10^{-2} A/cm criterion was not maintained over long times given the strong repassivation tendencies of these alloys. Moreover, the 10^{-2} A/cm criterion may not be severe enough given the harsh critical crevice chemistry required.[38] Thus, it appears that individual metastable pits do not individually and in absence of global crevice chemistry changes

stabilize crevice propagation. Stabilization did not occur in cases where I/r approached 10^{-2} A/cm indicating that the properties of individual events do not lead to crevice stabilization from perspective of local acidification and attainment of a critical crevice solution.

Instead, it is rationalized each event may contribute to a local chemistry change necessary to attain the severity of the critical crevice solution.[50] This does require that pit events occur close together in time and space. The latter is observed in Figures 12 and 13. Local acidification still continues as the result of increased passive dissolution rate as well as focused metastable pitting. Assuming coalescence of metastable pit sites along the perimeter of the crevice at a depth, x_{crit}, from the crevice mouth and a metastable event rate that is inversely proportional to time (Figure 6 and Figure 7), anodic charge accumulation (neglecting transport away from the pit site) increases with time according to Figure 21. Thus, the contribution to accumulated anodic charge (and thus metal cation hydrolysis) due to metastable pitting is much larger than charge accumulated due to passive dissolution current densities of 10^{-6} and 10^{-4} A/cm^2. However, with increasing accumulated charge due to metastable pit coalescence, local acidification occurs due to instantaneous hydrolysis reactions, leading to a passive current density that is an increasing function of time[38] (i.e., an increasing function of the cumulative number of metastable pits). Therefore, local acidification is primarily brought about by the formation of metastable pits in crevices when the passive current density is initially low. Local acidification then can be rationalized to continue due to an increased passive current density. In summary, the role of metastable pitting in crevices is most consistent with focused generation of hydrolyzable cations to augment the supply of hydrolyzable ions by passive dissolution.

Influence of Alloying and Microstructure on Crevice and Pitting Corrosion Initiation Sites

The metastable pitting properties of stainless steels and Ni-Cr-Mo alloys have been examined to determine the influence of alloying additions on event rates, values for peak integrated charge, I/r ratios, and peak shapes. Kobayashi, et al., examined the effects of Cr and Mo additions on small pit nucleation events in Fe-Cr alloys where the detection limit of the current was 2 pA.[14] Their results indicated that pit nucleation event rates decrease with increasing Cr and to a lesser extent, Mo content. However, the researchers concluded that this relationship may be affected by the current detection limit and that nucleation events may exist below this detection limit. In addition, peak heights and peak widths were found to decrease with increasing Cr and Mo content. Moreover, examination of the peak shapes revealed that growth times decrease with increasing Cr and to a lesser extent, Mo content. However, there was no effect of alloying additions of Cr and Mo on repassivation times. Therefore, the results suggest that Cr and Mo additions lead to an earlier start of repassivation but do not affect repassivation kinetics. The alloys considered in this study, 625 and 22, have equivalent Cr concentrations (approximately 21.6 wt.%) but slightly different Mo concentrations. The Mo concentrations for alloys 625 and 22 are 9.0 and 12.9 wt.%, respectively. However, recall from Table 3 that Cr equivalencies for alloys 625 and 22 are approximately 50 and 62, respectively. Examination of cumulative probability plots for peak heights (Figure 8), values for peak integrated charge (Figure 9), and I/r ratios (Figure 10) show that the distributions of these parameters do not differ significantly between the two alloys. This is consistent with the results of Kobayashi, et al., where only a small difference is seen among alloys with similar Cr concentrations but varying Mo concentrations.[14]

Williams, et al., examined the effect of alloyed Mo on metastable pitting for 316L and 304L stainless steels.[15] Their results showed that metastable pits in stainless steels containing Mo must grow to larger depths than those in stainless steels without Mo in order for the critical pit solution, which is more severe than for stainless steels without Mo, to be maintained. This argument is based on Galvele's i*r or I/r criterion for maintenance of a stable pit solution.[17] Ezuber and Newman also examined the influence of Mo on the metastable pitting behavior of 304 and 316 stainless steels showing that increasing Mo has the effect of shifting the distribution of metastable pit current densities to lower values at the same potential.[16] In separate studies, Stewart and Williams[51] and Baroux[18] examined the influence of manganese sulfide (MnS) inclusions on pit initiation. Stewart and Williams showed that S-rich inclusions act as pit initiation sites and that the transition to stability is a function of the size of these inclusions not the bulk S content of the alloy. Baroux examined the influence of manganese sulfide (MnS) inclusions on pit initiation as a function of chromium content. The results showed that MnS inclusions in stainless steels act as preferential sites for pit initiation. However, increasing Cr content causes the formation of (Mn, Cr) sulfides, thereby leading to an increased resistance to pit initiation. These mechanisms are unlikely for alloys 625 and 22 as the heat treatments of these alloys prevents the formation of inclusions that would act as susceptible pit initiation sites.[21, 22] Hence, the most likely difference in metastable pit event rates is traceable to Mo and W.

Relationship between Metastable Pit Sites and Stable Crevice Corrosion

The relationship between surface morphology and electrochemical signal was examined through serial removals of crevice corrosion samples at anodic charges corresponding to

occurrence of metastable pitting events in crevices only, the initiation of stable crevice corrosion, and the propagation of stable crevice corrosion (Figure 4).

Assuming that each event forms a hemispherical pit site within the crevice region, surface metrology studies at an accumulated anodic charge of 0.005 C, corresponding to metastable pitting events in crevices, reveal that initial crevice corrosion damage may evolve through the coalescence of a band of metastable pit sites formed at a critical depth, x_{crit}. Figure 12 and Figure 13 reveal that the structure of surface damage is a narrow band of shallow penetration depth along the outer edge of the crevice region. This is seen for both alloys. The narrow band can be justified given the need for both high potential and an aggressive chemistry to cause the formation of metastable events on Ni-Cr-Mo alloys. At positions deeper into the crevice, where IR drop is more significant leading to lower potentials, metastable events may not occur, despite the possibility of a more aggressive chemistry according to chemistry change models for crevice corrosion stabilization.[5, 17] However, the chemistry may not be more severe if cathodic focusing occurs.[28] Either situation may lead to the crevice geometry seen in Figure 12 and Figure 13. Thus, the band could be rationalized as a trade off between the location of highest potential and most severe chemistry. In addition, the narrow band indicates that crevice corrosion is controlled by chemistry change, which causes an increase in I_{pass}, thus causing an increase in the ohmic potential drop. If a single event satisfied the IR>IR* criterion, it would be expected that crevice corrosion would propagate radially from the metastable pit site and not in the narrow band as observed for alloys 625 and 22.

Just after the initiation of stable crevice corrosion (Figure 14), the morphology of the crevice site is characterized by a large depth of penetration near the crevice mouth and shallow attack at distances farther into the crevice region. This is typical of the morphology of a crevice

corroded region and is consistent with ohmic models as well as chemistry change models that consider cathodic focusing.[10, 28] In addition, a region of etch attack can be seen, on the outer edge of the crevice region before the metastable pit band, which corresponds to grain boundary attack suggesting acidification of the environment. The average grain size of 625 is 22 μm, while the average grain size of 22 is 45 μm.[46] These sizes are on the order of the grain sizes shown in the etch-attacked region indicating that the assumption of intergranular attack is valid.

In addition, comparison of alloys 625 and 22 indicates that for similar charge accumulation, the depth of penetration is smaller for alloy 22 than for 625. This is also seen after an accumulated charge of 0.02 C corresponding to the propagation of stable crevice corrosion. This indicates that crevice corrosion propagates laterally for alloy 22 spreading to new areas, while for 625, crevice corrosion leads to a large depth of penetration at a limited number of sites. Thus propagation is more severe for 625.

Comparison of surface metrology studies with electrochemical studies reveals that the properties associated with metastable pitting in crevices are similar for both alloys in terms of peak heights, values for peak integrated charge, and I/r ratios, as well as in the extent of surface damage caused by the coalescence of metastable pit sites (i.e., the extent of damage after a charge accumulation of 0.005 C). However, metastable event rates are higher for 625 than for alloy 22. Alloy 625, with higher metastable event rates and a less severe critical crevice solution as compared to alloy 22 should stabilize at lower potential-temperature conditions compared to alloy 22.[2] Moreover, the impact of a given number of metastable pits should be more severe as seen in Figure 5.

CONCLUSIONS

1. There is an inverse relationship between the cumulative number of metastable events and crevice stabilization potentials determined potentiodynamically.

2. Metastable corrosion event rates are higher for 625 than for alloy 22 at the same temperature and applied potential. In addition, increasing applied potential and temperature has the effect of increasing metastable event rates for both alloys. However, applied potential and temperature do not have strong effects on properties of individual metastable pits such as peak integrated charge and I/r ratio.

3. The role of metastable pitting in crevice stabilization is not certain but appears most consistent with generation of more hydrolyzable cations at a focused location in a crevice that augments the supply of hydrolyzable cations via passive dissolution. From this perspective, the greater number of events on alloy 625 at each temperature contributes to understanding the overall greater crevice susceptibility of this alloy compared to alloy 22. Individual metastable events do not appear to supply sufficient ohmic voltage drop to stabilize crevice attack. Nor do they individually appear to form and maintain critical crevice solutions in the absence of more global acidification within the crevice. Given these findings, it is also possible to rationalize why similarity of the properties of individual events on alloys 625 and 22 is not important to the stabilization process.

4. Surface metrology studies show that the depth of crevice corrosion attack is greater for 625 than for alloy 22.

5. Through surface metrology studies and assuming that each metastable event forms a small hemispherical pit, it can be concluded that crevice corrosion begins through the coalescence

of metastable pit sites at a critical distance within the crevice. The justification for this distance can be rationalized and the narrow band formed is quite evident.

ACKNOWLEDGEMENTS

REFERENCES

1. A. J. Sedriks, Corrosion of Stainless Steels (New York: John Wiley & Sons, 1996).
2. B. A. Kehler, G. O. Ilevbare, J. R. Scully, Corrosion 57, 12 (2001): p. 1042.
3. E. L. Hibner, "Modification of Critical Crevice Temperature Test Procedures for Nickel Alloys in a Ferric Chloride Environment," CORROSION/86 (1986).
4. N. J. Laycock, J. Stewart, R. C. Newman, Corrosion Science 39, 10-11 (1997): p. 1791.
5. J. W. Oldfield, W. H. Sutton, Br. Corros. J. 13, 1 (1978): p. 13.
6. J. W. Oldfield, W. H. Sutton, Br. Corros. J. 15, 1 (1980): p. 31.
7. S. E. Lott, R. C. Alkire, J. Electrochem. Soc. 136, 4 (1989): p. 973.
8. R. C. Alkire, S. E. Lott, J. Electrochem. Soc. 136, 11 (1989): p. 3256.
9. H. W. Pickering, "A Critical Review of IR Drops and Electrode Potentials Within Pits, Crevices, and Cracks," Advances in Localized Corrosion (National Association of Corrosion Engineers, 1987).
10. B. De Force, H. W. Pickering, JOM 47, 9 (1995): p. 22.
11. H. W. Pickering, Corrosion Science 29, 2/3 (1989): p. 325.
12. Y. Xu, H. W. Pickering, J. Electrochem. Soc. 140, 3 (1993): p. 658.
13. L. Stockert, H. Boehni, "Metastable Pitting Processes and Crevice Corrosion on Stainless Steels," Advances in Localized Corrosion (National Association of Corrosion Engineers, 1987).
14. Y. Kobayashi, S. Virtanen, H. Boehni, J. Electrochem. Soc. 147, 1 (2000): p. 155.
15. D. E. Williams, J. Stewart, P. H. Balkwill, "Nucleation, Growth, and Stability of Micropits in Stainless Steel," Critical Factors in Localized Corrosion II (1992).
16. H. Ezuber, R. C. Newman, "Growth-Rate Distribution of Metastable Pits," Critical Factors in Localized Corrosion (The Electrochemical Society, Inc., 1991).
17. J. R. Galvele, J. Electrochem. Soc. 123, 4 (1976): p. 464.
18. B. Baroux, "Further Insights on the Pitting Corrosion of Stainless Steels," in Corrosion Mechanisms in Theory and Practice, eds. P. Marcus and J. Oudar (New York: Marcel Dekker, Inc., 1995), p. 265.
19. R. B. Rebak, P. Crook, Advanced Materials & Processes, February 2000 (2000): p. 37.
20. G. E. Gdowski (1991) Survey of Degradation Modes of Four Nickel-Chromium-Molybdenum Alloys. Livermore, CA: KMI Energy.
21. (2002) Inconel Alloy 625. Huntington, WV: Special Metals Corporation.
22. (2003) Inconel Alloy 22. Huntington, WV: Special Metals Corporation.
23. F. M. G. Wong (2003) Summary of Alloy 22 Aging and Phase Stability Studies. In *DOE OCRWM/BES Corrosion Workshop* Bethesda, MD: LLNL.
24. (1998) Viability Assessment of a Repository at Yucca Mountain: Volume 4. License Application Plan and Costs. Las Vegas: U.S. Department of Energy (Office of Civilian Radioactive Waste Management).
25. (1998) Drip Shields LA Reference Design Feature Evaluation #2. Las Vegas: TRW Environmental Safety Systems, Inc.
26. J. R. Scully, S. T. Pride, H. S. Scully, J. L. Hudson, "Some Correlations Between Metastable Pitting and Pit Stabilization in Metals," (The Electrochemical Society, 1996).
27. S. T. Pride, J. R. Scully, J. L. Hudson, J. Electrochem. Soc. 141, 11 (1994): p. 3028.
28. K. C. Stewart (1999) Crevice Corrosion by Cathodic Focusing. In *Department of Materials Science and Engineering* Charlottesville: University of Virginia.
29. H. Boehni, F. Hunkeler, "Growth Kinetics and Stability of Localized Corrosion Processes," Advances in Localized Corrosion (National Association of Corrosion Engineers, 1987).
30. T. Shibata, T. Takeyama, Corrosion 33, 7 (1977): p. 243.
31. G. A. Henshall, Journal of Nuclear Materials 195 (1992): p. 109.
32. G. S. Frankel, L. Stockert, F. Hunkeler, H. Boehni, Corrosion 43, 7 (1987): p. 429.
33. G. T. Burstein, P. C. Pistorius, S. P. Mattin, Corrosion Science 35, 1-4 (1993): p. 57.
34. F. Sato, R. C. Newman, Corrosion 54, 12 (1998): p. 955.
35. P. C. Pistorius, G. T. Burstein, Phil. Trans. R. Soc. Lond. A 341 (1992): p. 531.
36. "Standard Practice for Preparing, Cleaning, and Evaluating Corrosion Test Specimens, Designation G 1-90," in Annual Book of ASTM Standards, (Philadelphia: American Society for Testing and Materials, 1990)
37. D. A. Jones, Principles and Prevention of Corrosion (Englewood Cliffs, NJ: Prentice-Hall, Inc., 1992).
38. R. S. Lillard, M. P. Jurinski, J. R. Scully, Corrosion 50, 4 (1994): p. 251.

39. J. Charles, J. P. Audouard, M. Verneau, "Metallic Answers for F.G.D. Systems (Paper 480)," Corrosion/98 (National Association of Corrosion Engineers, 1998).

40. Grounding and Shielding in Electrochemical Instrumentation - Some Basic Considerations (Application Note G-2). Princeton, NJ: EG&G Princeton Applied Research - Analytical Instrument Division, pp 1.

41. CorrWare. Southern Pines, NC: Scribner Associates, Inc.

42. T. T. Lunt (2000) PeakFindC. Charlottesville, VA.

43. A. Turnbull, Brit. Corr. J. 28, 4 (1993): p. 297.

44. G. T. Burstein, S. P. Mattin, "The Nucleation and Early Stages of Growth of Corrosion Pits," Electrochemical Society (Electrochemical Society Proceedings, 1995).

45. R. S. Lillard, J. Electrochem. Soc. 148, 1 (2001): p. B1.

46. "Standard Test Methods for Determining Average Grain Size, Designation E 112-88," in Annual Book of ASTM Standards, Vol. ASTM E112 (Philadelphia: American Society for Testing and Materials, 1988)

47. P. O. Gartland (1988) A Mathematical Model of Crevice Corrosion for Fe-Ni-Cr-Mo Alloys in Chloride Solutions. SINTEF.

48. B. A. Shaw, P. J. Moran, P. O. Gartland, Corrosion Science 32, 7 (1991): p. 707.

49. J. Newman, Electrochemical Systems (Englewood Cliffs, NJ: Prentice Hall Publishing, 1973).

50. H. S. Isaacs, "Diffusional Processes in Crevice Corrosion," Research Topical Symposium - Localized Corrosion (National Association of Corrosion Engineers, 2001).

51. J. Stewart, D. Williams, Corrosion Science 33, 3 (1992): p. 457.

31

TABLES

Table 1. Measured chemical composition (weight percent) of alloys 625 and 22. For comparison, consider that stainless steels typically have 2 wt.% Mn and 0.02 wt.% S.

Element	625	22
C	0.03	0.01
Cr	21.08	21.55
Co	0.07	1.07
Fe	3.61	3.83
Mn	0.09	0.22
Mo	8.88	13.05
Ni	Balance	Balance
P	0.01	0.01
Si	0.22	0.01
S	0.00	0.00
W	-	2.82
V	-	0.15
Al	0.19	-
Nb+Ta	3.36	-
Ti	0.26	-

Table 2. Heat treatments specifications and measured mechanical properties for alloys 625 and 22.

	625	22
Heat Treatment	Mill Annealed at Minimum of 871°C	Solution Annealed at Minimum of 1121°C
Micrograin Size Number	8.0-9.0	5.0-6.0
Hardness	96.5	91.5
Tensile Strength (ksi)	135.8	118.3
Yield Strength (ksi)	74.7	60.4
Elongation in 2 in (%)	46.2	58.0

Table 3. Calculated values for pitting resistance equivalency numbers (PREN), modified pitting resistance equivalency numbers (PRE'), and chromium equivalencies for alloys 625 and 22.

	625	22
PREN	50.38	64.60
PRE'	50.38	73.91
Cr Equivalency	49.75	62.16

FIGURES
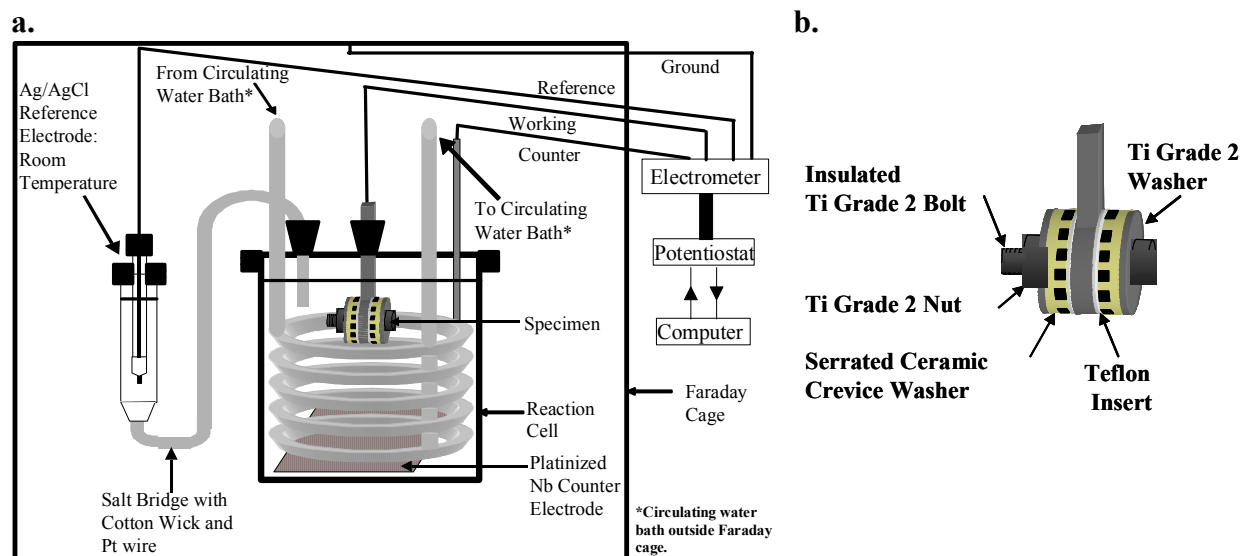
Figure 1. (a) Test setup for measurement of metastable pitting behavior inside crevices. Background noise was minimized by performing all experiments in a Faraday cage. Thermal noise was minimized by isolating the cell from the heat source by circulating heated water through a coil placed directly in the cell. The specimen as arranged in a multiple crevice assembly is shown in greater detail in (b). The face of the sample was placed inside a crevice assembly consisting of serrated ceramic multiple crevice formers with 12 plateaus each of area 0.06 cm^2 lined with polytetrafluoroethylene (PTFE) tape.
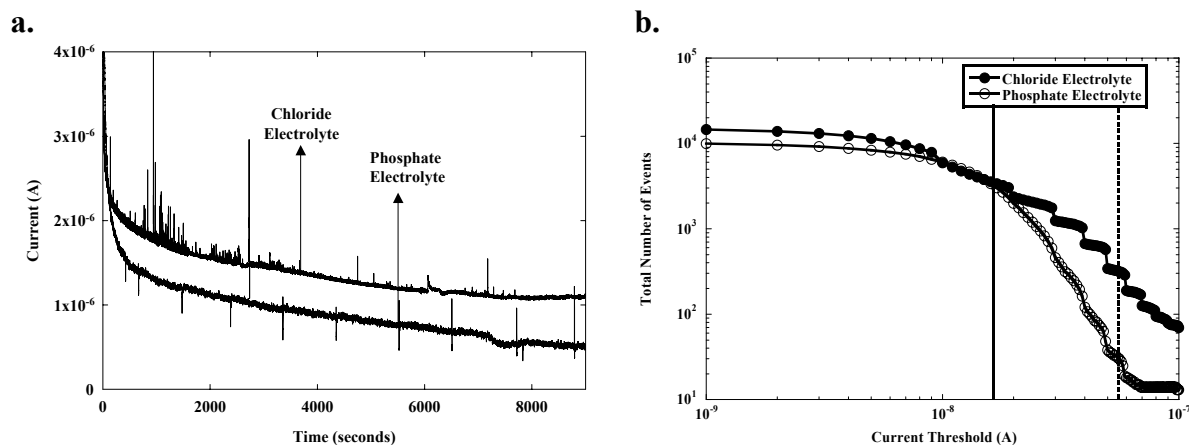
Figure 2. (a) Current versus time records for 625 in chloride and phosphate electrolytes at pH 2.75 and 95°C and (b) the corresponding results for total number of events versus current threshold. The solid vertical line in (b) indicates the current threshold at which the curves for the chloride and phosphate electrolytes begin to separate as the number of events counted that could be attributed to the background noise begins to decrease. The dotted vertical line indicates the current threshold at which the total number of events in the benign phosphate electrolyte was less than 10% of the total number of events in the chloride electrolyte. A current threshold of 56 nA was selected through this analysis.
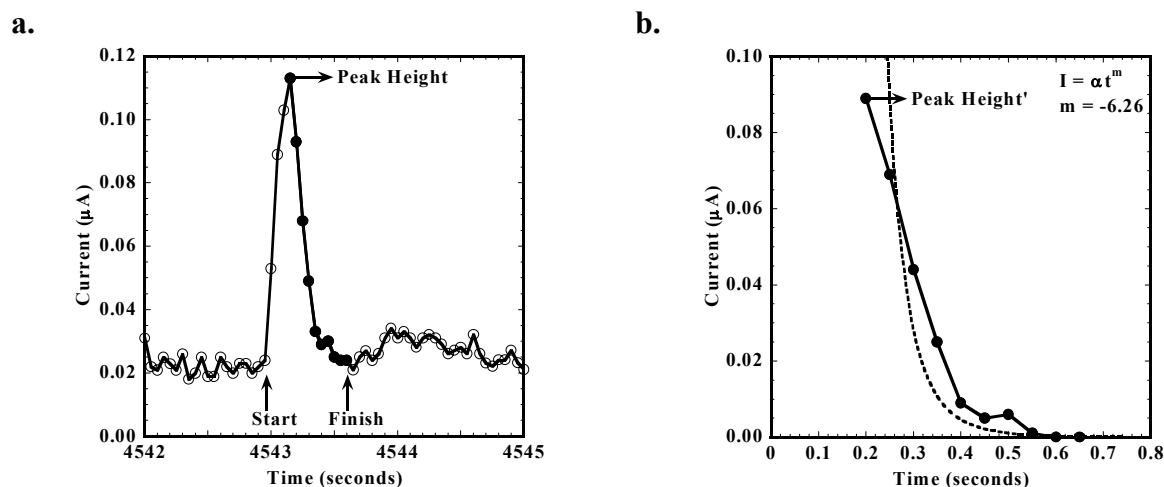
Figure 3. Examination of a metastable event showing (a) the entire event before baseline subtraction and (b) the repassivation stage after complete baseline subtraction with the corresponding power law fit. Initiation of growth, corresponding to time zero in the lifetime of the event, is indicated by the start arrow. Completion of the event is indicated by the finish arrow. This is the point at which the current returns to or falls below the level of the passive current, which is defined as the current at the time of initiation. Peak height' in (b) corresponds to the peak height indicated in (a) minus the passive current. The repassivation stage is denoted by ●.
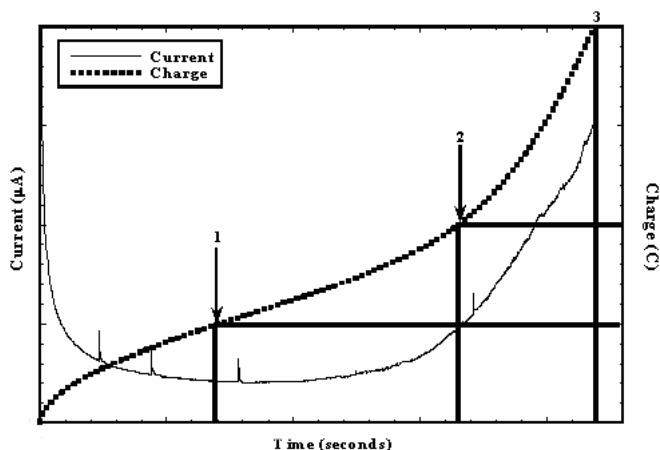
Figure 4. A sample current versus time record with corresponding charge versus time relationship showing the approximate positions of serial removals for surface metrology studies. 1 corresponds to metastable corrosion and a charge collection of 0.005 C. 2 and 3 correspond to stable crevice corrosion just after initiation (0.01 C) and after continued propagation (0.02 C), respectively. Note that the samples used for surface metrology studies were in a polished condition. Therefore, induction times for stable crevice corrosion differ from those for the as-received samples.
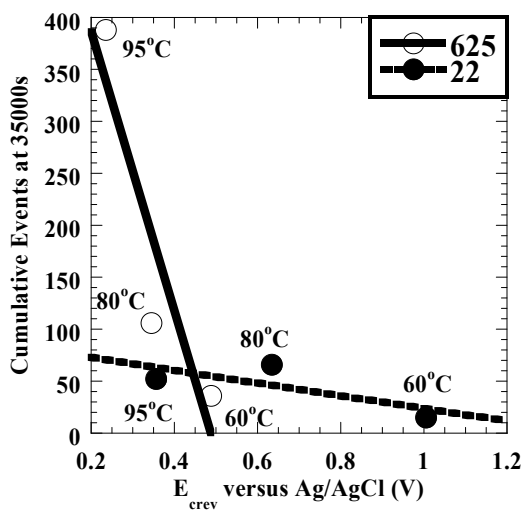
a.
b.
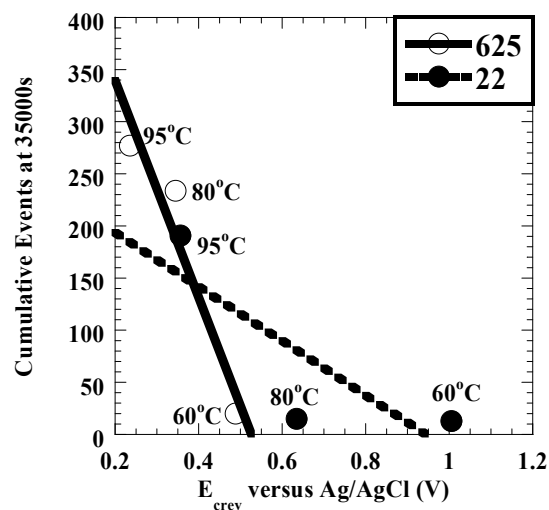
Figure 5. Cumulative number of metastable events at 35000 seconds versus calculated E_{crev} values for alloys 625 and 22 at applied potentials of (a) +5 $mV_{Ag/AgCl}$ and (b) -25 $mV_{Ag/AgCl}$. Values for cumulative events were not normalized to sample area.

a.
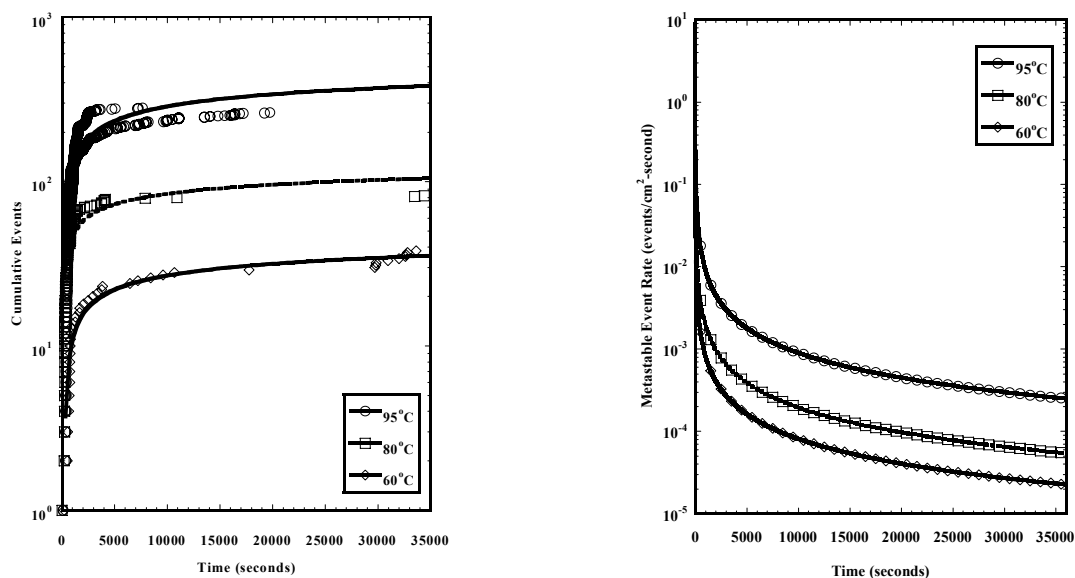
b.
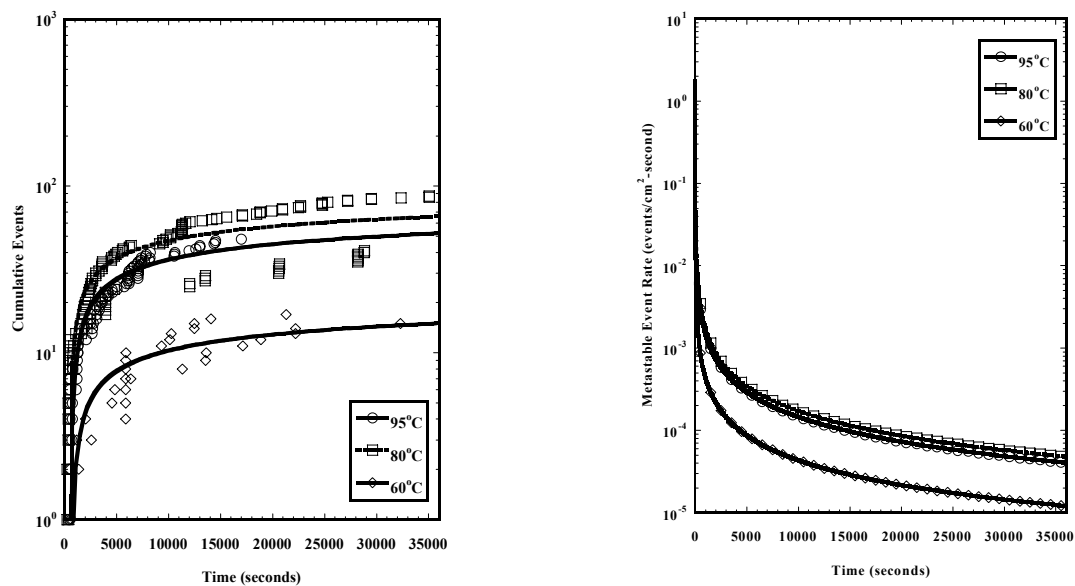
Figure 6. Cumulative number of metastable events versus time with corresponding metastable event rate curves for (a) alloy 625 and (b) alloy 22 specimens with a surface finish of 2-4 μm (average roughness) at an applied potential of +5 mV$_{Ag/AgCl}$. The temperatures for collection of the current-time records were 95°, 80°, and 60°C. Average values for replicate specimens are by given solid and dashed lines. The total sample area was 8.5 cm^2, while the area under the crevice formers was 1.44 cm^2. Metastable event rates were normalized to the total sample area. Values for cumulative events were not normalized to sample area.

a.
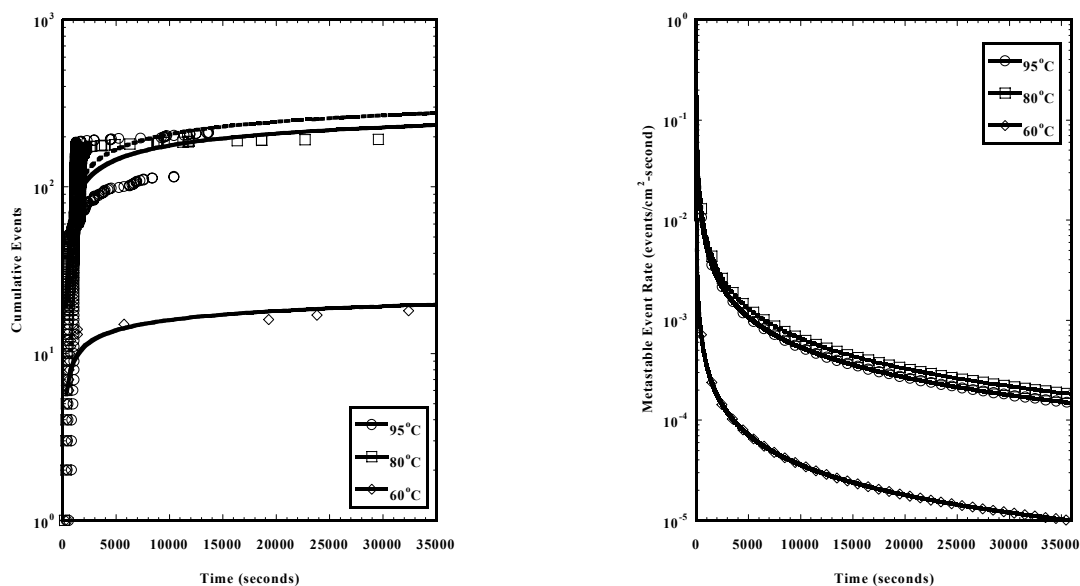
b.
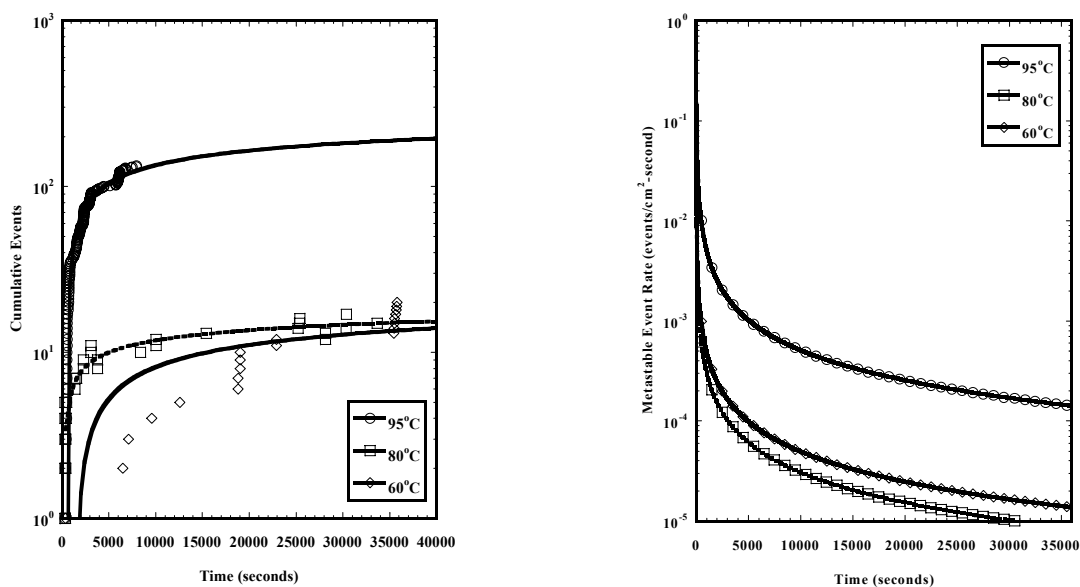
Figure 7. Cumulative number of metastable events versus time with corresponding metastable event rate curves for (a) alloy 625 and (b) alloy 22 specimens with a surface finish of 2-4 μm (average roughness) at an applied potential of -25 mV$_{Ag/AgCl}$. The temperatures for collection of the current-time records were 95°, 80°, and 60°C. Average values for replicate specimens are given by solid and dashed lines. The total sample area was 8.5 cm^2, while the area under the crevice formers was 1.44 cm^2. Metastable event rates were normalized to the total sample area. Values for cumulative events were not normalized to sample area.
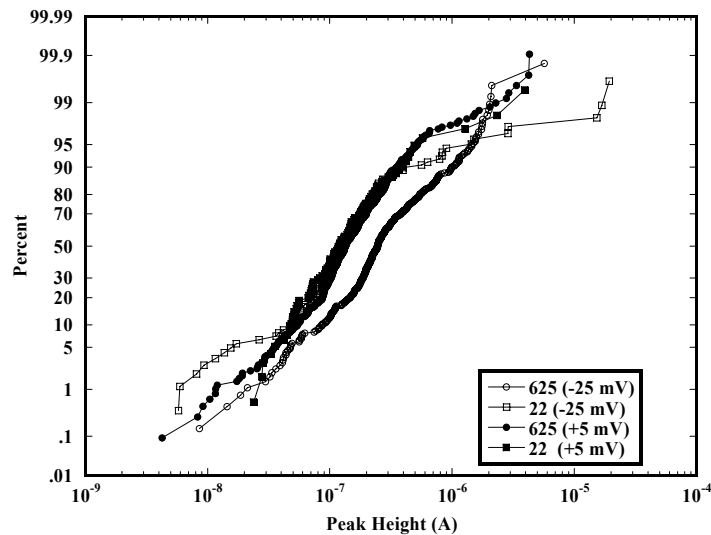
Figure 8. Cumulative probability plots of metastable peak heights for alloy 625 and alloy 22 specimens with a surface finish of 2-4 μm (average roughness) at 95°C at applied potentials of +5 mV$_{Ag/AgCl}$ and -25 mV$_{Ag/AgCl}$.
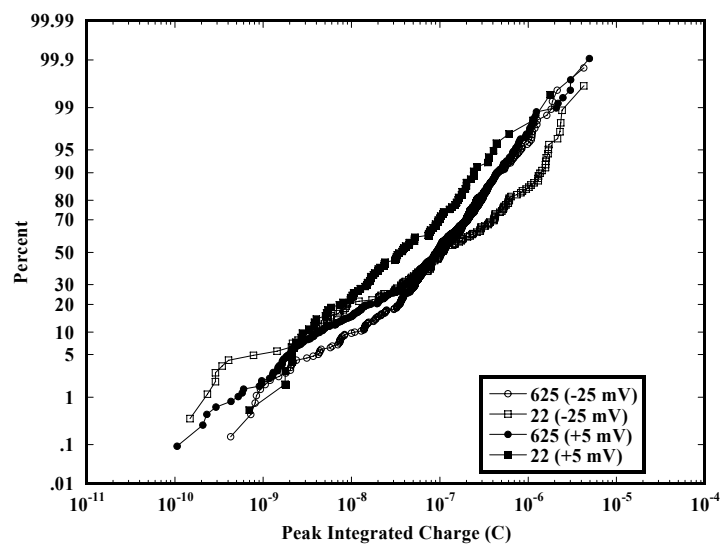
Figure 9. Cumulative probability plots of values for peak integrated charge for alloy 625 and alloy 22 specimens with a surface finish of 2-4 μm (average roughness) at 95°C at applied potentials of +5 mV$_{Ag/AgCl}$ and -25 mV$_{Ag/AgCl}$.
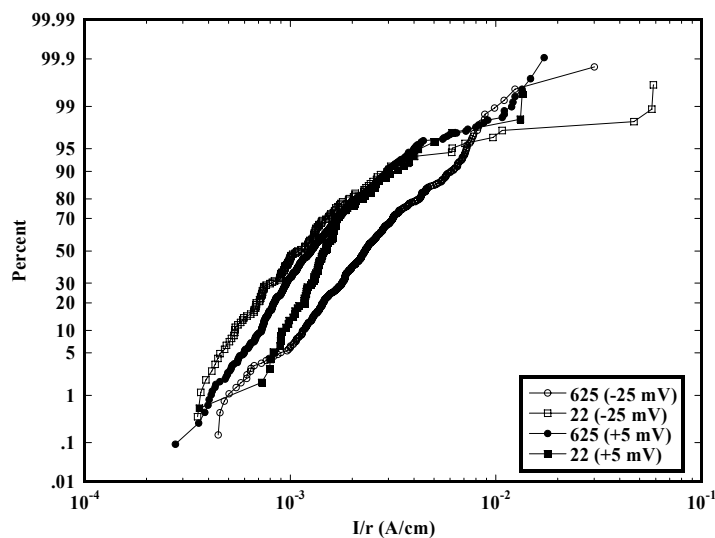
Figure 10. Cumulative probability plots of metastable I/r ratios for alloy 625 and alloy 22 specimens with a surface finish of 2-4 μm (average roughness) at 95°C at applied potentials of +5 mV$_{Ag/AgCl}$ and -25 mV$_{Ag/AgCl}$. r values were calculated assuming a hemispherical geometry.
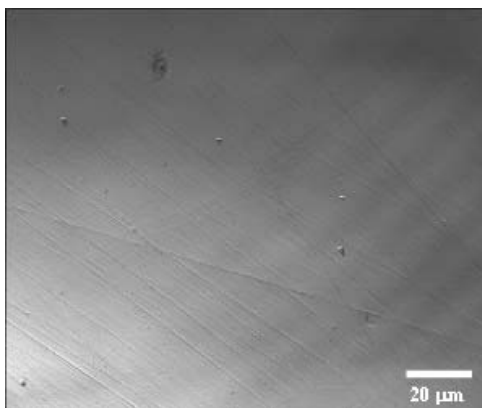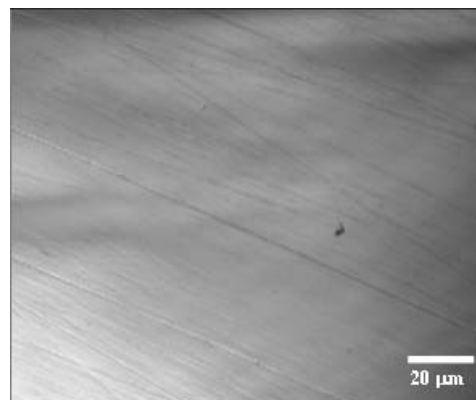
Figure 11. CLSM reflected light intensity maps of (a) alloy 625 and (b) alloy 22 after successive polishing to a 1 μm diamond finish. Note the presence of small dimples in the polished surface. CLSM images of polished surfaces are used to distinguish surface defects from the results of metastable events and stable crevice corrosion.

a.

b.
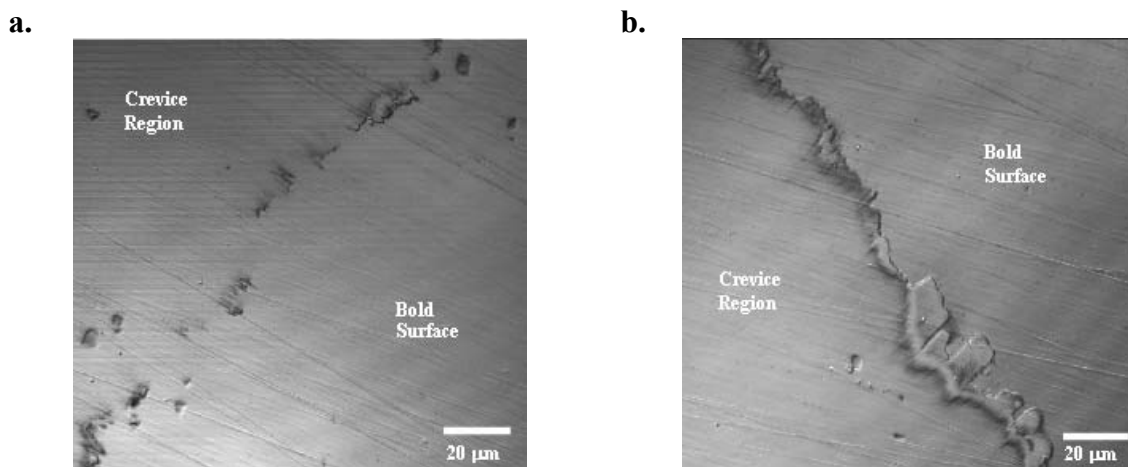
Figure 12. CLSM reflected light intensity maps of alloy 625 after an accumulated charge of 0.005 C showing (a) areas of attack due to individual crevice corrosion events and (b) further attack at the outer edge of the crevice region due to apparent coalescence of these metastable pits. Electrodes were polarized to +5 mV$_{Ag/AgCl}$ at 95°C. The crevice region is defined as the area created by the deformable PTFE insert in conjunction with the ceramic multiple crevice former. The bold electrode surface is also indicated.

a.

b.
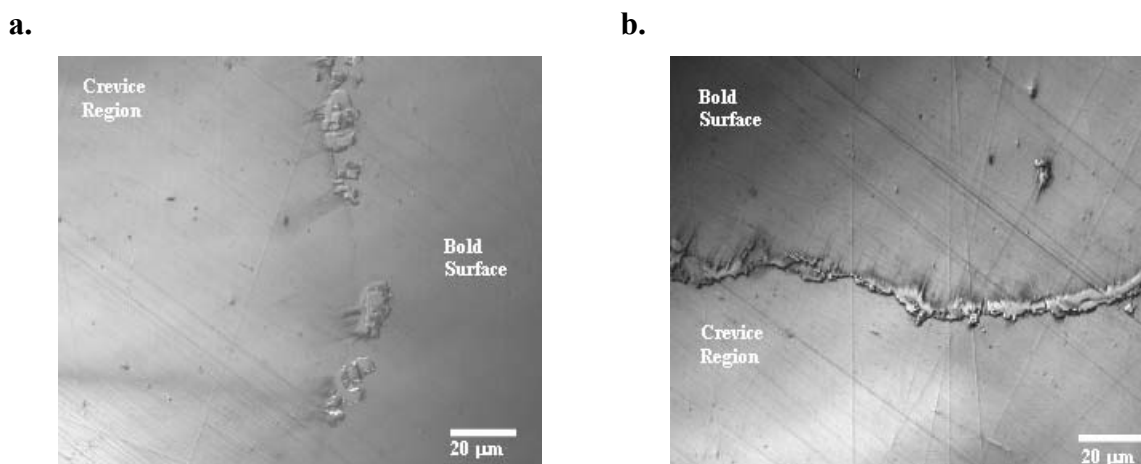
Figure 13. CLSM reflected light intensity maps of alloy 22 after an accumulated charge of 0.005 C showing (a) areas of attack due to individual crevice corrosion events and (b) further attack at the outer edge of the crevice region due to apparent coalescence of these metastable pits. Electrodes were polarized to +5 mV$_{Ag/AgCl}$ at 95°C in pH 2.75 (10:1) electrolyte. The crevice region is defined as the area created by the deformable PTFE insert in conjunction with the ceramic multiple crevice former. The bold electrode surface is also indicated.

a.
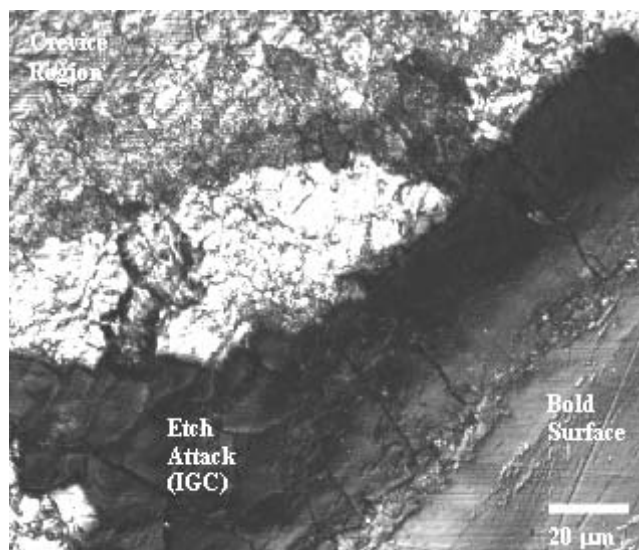
b.
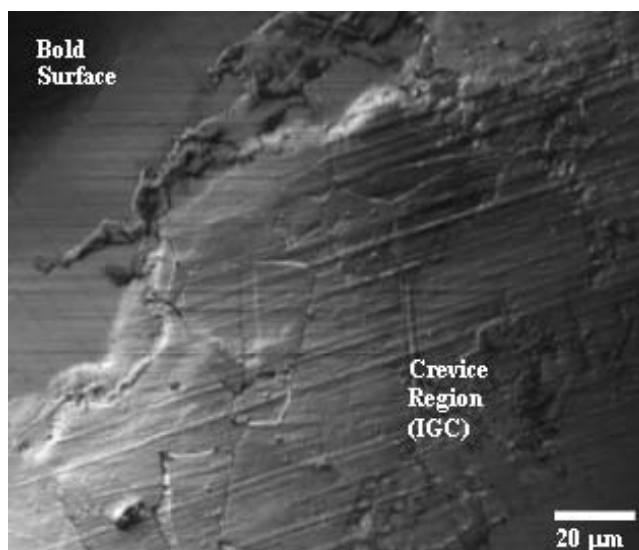
Figure 14. CLSM reflected light intensity maps of (a) alloy 625 and (b) alloy 22 after an accumulated charge of 0.01 C. The bold surface and the crevice region are indicated. The electrode was polarized to +5 mV$_{Ag/AgCl}$ at 95°C in pH 2.75 (10:1) electrolyte.
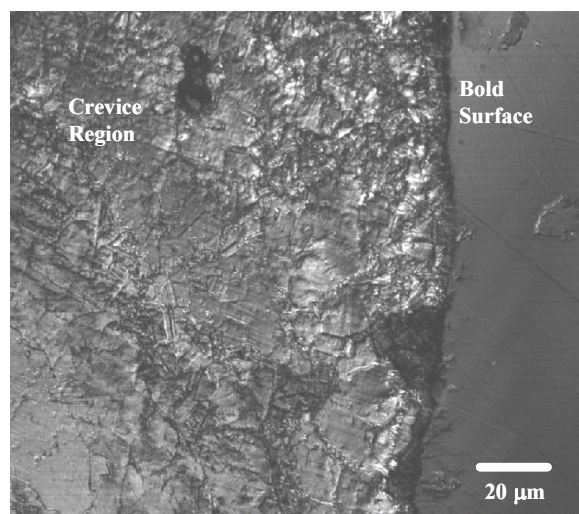
Figure 15. CLSM image of alloy 625 after an accumulated charge of 0.02 C showing a 2-D reflected light intensity map. The electrode was polarized to +5 mV$_{Ag/AgCl}$ at 95°C. The bold surface and the crevice region are indicated.

a.
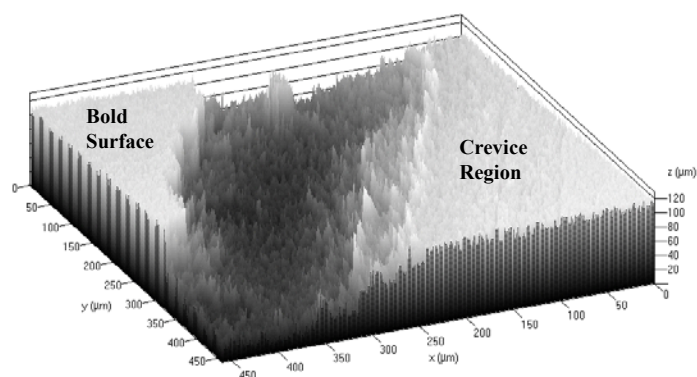
b.
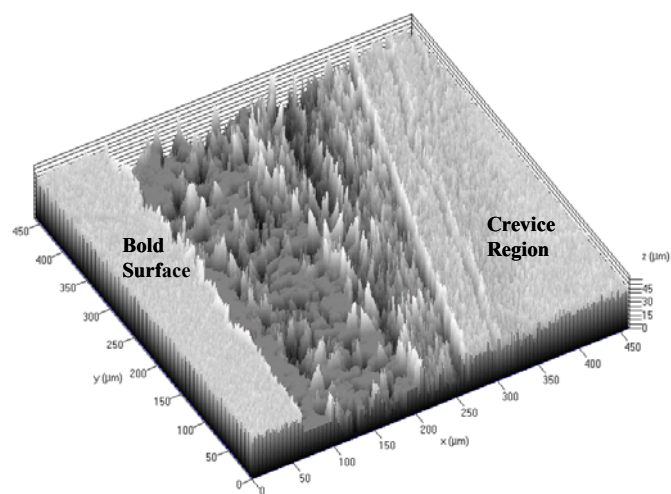
Figure 16. CLSM images of (a) alloy 625 and (b) alloy 22 after an accumulated charge of 4 C showing 3-D reflected light intensity maps. The electrodes were polarized to +400 $mV_{Ag/AgCl}$ at 95°C to allow for propagation of stable crevice corrosion. The 3-D depth profiles correspond to a maximum depth of penetration of approximately 120 μm and 45 μm for alloys 625 and 22, respectively.
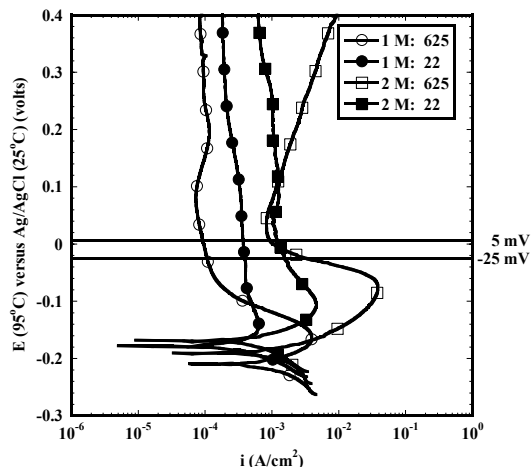
Figure 17. Anodic polarization scans of alloys 625 and 22 at 95°C in 1 M and 2 M HCl based simulated crevice solutions. Electrodes were wet ground to a 600 grit finish. Applied potentials of +5 mV$_{Ag/AgCl}$ and -25 mV$_{Ag/AgCl}$ used to examine metastable pitting in crevices are denoted to show the ohmic potential drop required for stabilization of crevice corrosion in aggressive crevice environments.
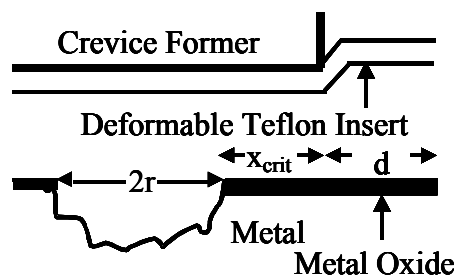

Figure 18. Multiple crevice assembly arrangement showing a view of crevice region defined by ceramic crevice former and deformable PTFE insert.
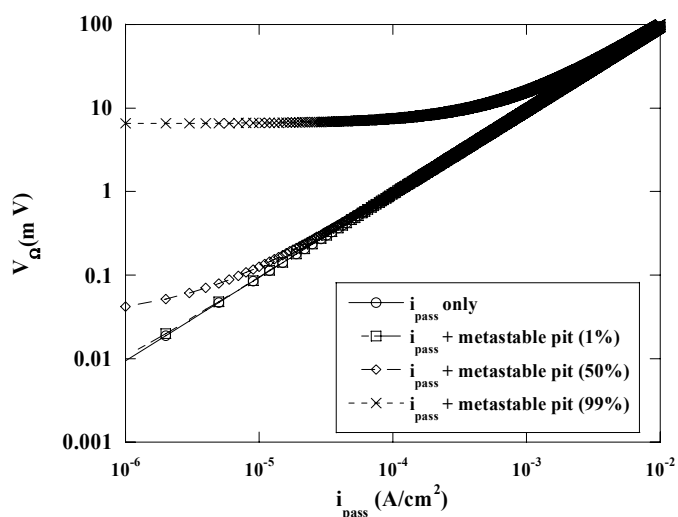

Figure 19. Ohmic potential drop due to contributions from passive current density only and passive current density plus the formation of metastable pits.
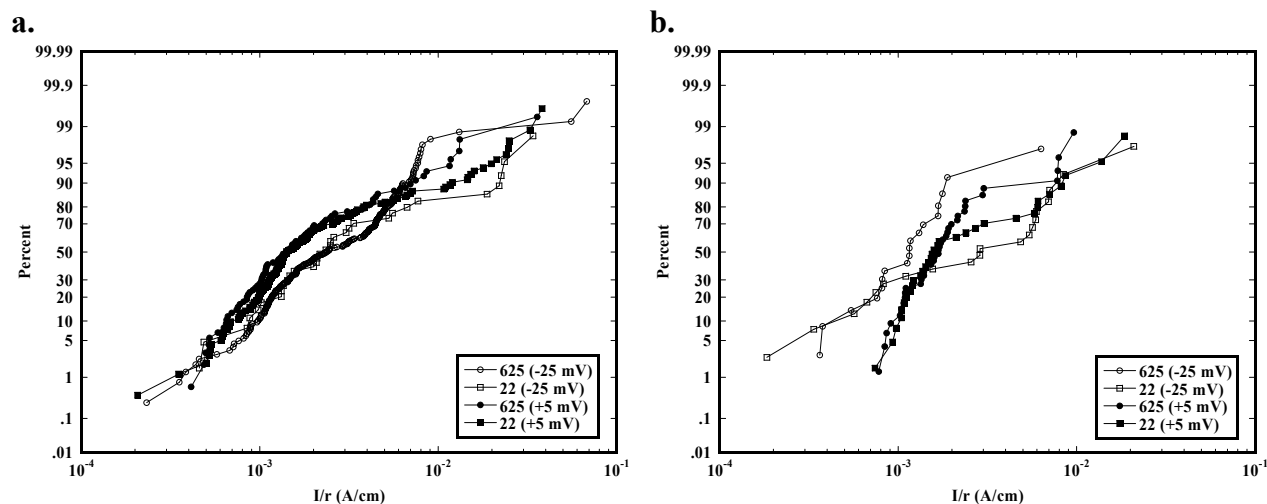
a.

b.

Figure 20. Cumulative probability plots of metastable I/r ratios for alloy 625 and alloy 22 specimens with a surface finish of 2-4 μm (average roughness) at (a) 80°C and (b) 60°C at applied potentials of +5 mV$_{Ag/AgCl}$ and -25 mV$_{Ag/AgCl}$. r values were calculated assuming a hemispherical geometry.
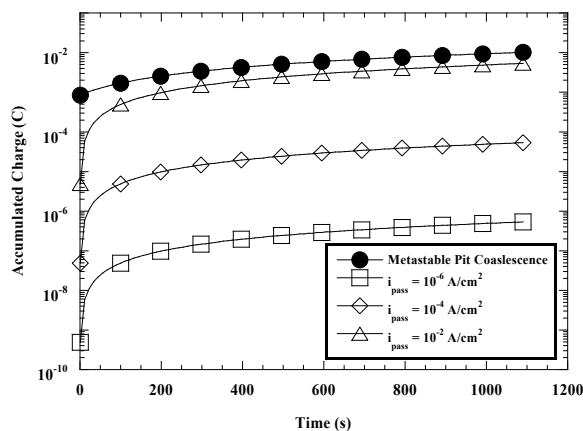

Figure 21. Accumulated charge versus time due to metastable pit coalescence and passive current density focused along the perimeter of the crevice at a depth, x_{crit}, from the crevice mouth. Calculations for accumulated charge due to metastable pit coalescence assumed metastable pits of 5 μm radius and an accumulated charge of 10^{-5} C/pit. Calculations for accumulated charge due to passive current density assumed passive current densities of 10^{-6}, 10^{-4}, and 10^{-2} A/cm^2 that were constant with time.